



This is a repository copy of *Study of the machining induced damage in UD-CFRP laminates with various fibre orientations : FE assessment.*

White Rose Research Online URL for this paper:
<http://eprints.whiterose.ac.uk/161417/>

Version: Published Version

Proceedings Paper:

Cepero-Mejías, F., Curiel-Sosa, J.L., Kerrigan, K. orcid.org/0000-0001-6048-9408 et al. (1 more author) (2020) Study of the machining induced damage in UD-CFRP laminates with various fibre orientations : FE assessment. In: *Procedia CIRP. 5th CIRP Conference on Surface Integrity (CSI 2020)*, 01-05 Jun 2020, Arrasate, Spain (online conference). Elsevier , pp. 366-371.

<https://doi.org/10.1016/j.procir.2020.02.028>

Reuse

This article is distributed under the terms of the Creative Commons Attribution-NonCommercial-NoDerivs (CC BY-NC-ND) licence. This licence only allows you to download this work and share it with others as long as you credit the authors, but you can't change the article in any way or use it commercially. More information and the full terms of the licence here: <https://creativecommons.org/licenses/>

Takedown

If you consider content in White Rose Research Online to be in breach of UK law, please notify us by emailing eprints@whiterose.ac.uk including the URL of the record and the reason for the withdrawal request.



eprints@whiterose.ac.uk
<https://eprints.whiterose.ac.uk/>

5th CIRP CSI 2020

Study of the machining induced damage in UD-CFRP laminates with various fibre orientations: FE assessment

F. Cepero-Mejías^{a,b*}, J.L. Curiel-Sosa^b, K. Kerrigan^c, V.A. Phadnis^d

^aIndustrial Doctorate Centre in Machining Science, The University of Sheffield, S1 3JD, UK.

^bDepartment of Mechanical Engineering, The University of Sheffield, S1 3JD, UK.

^cAdvanced Manufacturing Research Centre with Boeing, University of Sheffield, Advanced Manufacturing Park, Wallis Way, Catcliff, Rotherham, S60 5TZ, United Kingdom.

^d3M, Bracknell RG12 8HT, United Kingdom

* Corresponding author. Tel.: +44-793-881-2394; E-mail address: fmcepero1@sheffield.ac.uk

Abstract

Finite elements (FE) provide an excellent and low-cost approach in the assessment of composite machining induced damage. This article is focused on the evaluation of the damage underlying the machined surface through the development of a novel 3D FE model in composite machining. Sub-surface damage of UD-CFRP with fibre orientations from 0° to 90° is evaluated. An algorithm to assess composite damage evolution and chip formation is inserted via user-defined subroutine. Damage initiation is determined using Hashin's failure criteria for fibre damage modes, while matrix damage modes are assessed via Puck's failure criteria. Subsequent damage evolution is modelled using an energy-based linear damage degradation law. Numerical results reveal relevant advances in the prediction of the damage induced underlying the machined surface for fibre orientations from 60° to 90° obtained in previous investigations.

© 2020 The Authors. Published by Elsevier B.V.

This is an open access article under the CC BY-NC-ND license (<http://creativecommons.org/licenses/by-nc-nd/4.0/>)

Peer-review under responsibility of the scientific committee of the 5th CIRP CSI 2020

Keywords: Machining; Finite element; Composite; Subsurface damage

1. Introduction

In the last decade, the use of composite components has been exponentially increased in industrial applications due to their extraordinary capabilities to satisfy the high performance application demands. In particular, composite materials are highly demanded in aeronautical components owing their high strength-to-weight ratio allows significant weight savings. For example, the use of CFRP parts in the airframe of the aircraft Boeing 787 achieve a weight save around the 20% in comparison with conventional aluminum designs [1].

Despite composite components are manufactured in a near net shape, they usually require to be machined to satisfy the strict dimensional and structural requirements. Unfortunately,

factors such as the presence of high abrasive fibres or tough and low thermal conductivity resins generally occasion a rapid degradation of the cutting edges in high-speed machining applications [2]. As a result, the tool notched edge push the fibres instead of shearing them away increasing notably the damage underlying the machined surface [3]. Additionally, for fibre orientations perpendicular to the cutting direction the fibre bending is important and this induces an important increment of crack nucleation around the edges surfaces [4]. Therefore, the investigation of machining configurations to reduce this kind of problems is highly necessary.

Due to the high cost of CFRP components, tooling and machines, experimental investigations pose an expensive solution to address this matter. Subsequently, a finite element

analysis offers an attractive and cost-effective approach in composite machining. Currently, several works have developed FE analysis to study the subsurface damage in composite machining. Relevant investigations in this topic are summarised below.

Santiuste et al. [5] studied the chip formation and the machining induced damage in GFRP and CFRP laminates by means of FE simulations. This work concluded that CFRP laminates experience a fragile chip fracture with low machining induced damage, while GFRP laminates have a more ductile chip fracture with higher subsurface damage. In another investigation in the modelling of CFRP/Ti stack, Xu et al. [6] concluded that low feed rates and high cutting velocities reduce considerably the machining induced damage of CFRP components. Other researchers have conducted studies to determine the influence of cutter morphology on the machining induced damage. For instance, Zenia et al. [7] concluded that high fibre orientations and depth-of-cuts increase the subsurface damage, while increments of rake angles decrease the induced machining damage. More recently, Cepero-Mejías et al. [8] investigated the influence of different cutting parameters such as relief angle, rake angle and tool edge radius. It is concluded that tool wear until 50 μm and rake angle has not a clear influence in the subsurface damage, while high relief angles reduce significantly the machining induced damage.

Despite several analyses have been performed in the modelling of composite machining so far, most works have developed 2D FE models. This kind of models is still limited to study the machining of UD laminates avoiding more complex studies where laminate thickness takes a relevant role. For example, 3D FE models are required for the study of the machining of cross-ply laminates or to analyse the delamination caused during the machining between plies. Therefore, the development of accurate 3D FE models to predict the underlying damage becomes essential to guarantee an excellent final surface quality in composite machining.

This paper is focused on the development a novel 3D FE analysis of the underlying damage in the machining of CFRP laminates. For this purpose, a novel composite damage algorithm in composite machining is inserted via user-defined subroutine. Fibre and matrix damage initiation are calculated using the well-established composite failure criteria of Hashin and Puck, respectively. A linear energy based damage law is employed to degrade progressively the mechanical properties of the affected area; shear and matrix damages are limited to avoid numerical errors. Numerical results are compared with the results extracted from the 2D FE study developed by these authors [8] observing a good correlation in the subsurface damage. Higher machining induced damage predictions for fibre orientations between 60° and 90° are obtained in comparison with the aforementioned work; enhancing the quality of the numerical simulations because the subsurface damage was under predicted in the 2D FE study.

2. FE model characteristics

This work is performed using an explicit analysis in the numerical software Abaqus/CAE linked to well-known programming language software called FORTRAN. Using

this configuration a great customization of material behaviour is achieved with the use of a VUMAT user-defined subroutine. More details about how VUMAT subroutine employed here are offered in section 4.

Table 1. Cutting parameters modelled

Parameters	Values
Rake angle (°)	5
Relief angle (°)	6
Depth of cut (mm)	0.2
Tool edge radius (μm)	50
Fibre orientation (°)	0, 15, 30, 45, 60, 75 and 90

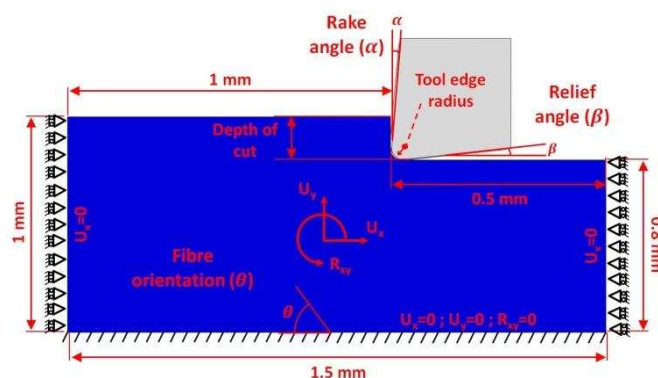


Fig. 1. Representation of model important parameters

As the simulations developed by Cepero et al. [8] are used in this work with purposed of proving the accuracy of the FE model analysed here, the same machining configuration simulated in this work will be employed. A visualisation of these machining parameters is offered in Fig 1, while the employed values are shown in Table 1. Finally, mechanical properties factors and strength of the CFRP laminate modelled in this investigation are illustrated in Tables 2 and 3, respectively.

Table 2. Mechanical properties of the CFRP laminate

E_1 (GPa)	$E_2 = E_3$ (GPa)	$G_{12} = G_{13}$ (GPa)	G_{23} (GPa)	$\nu_{12} = \nu_{13}$	ν_{23}
136.6	9.6	5.2	3.47	0.29	0.4

Table 3. Strength properties of the CFRP laminate. All units are in MPa

X_T	X_C	$Y_T = Z_T$	$Y_C = Z_C$	$S_{12} = S_{13} = S_{23}$
2720	1690	111	214	115

Specimens 1 mm height and 1.5 mm width are simulated to obtain accurate predictions with a reasonable computational cost. To achieve an accurate simulation of a real machining operation the bottom side of the specimen is fixed, while the lateral laminate edges the horizontal displacement is restricted, see Fig. 1. Finally, the out of plane displacement of the elements, in lateral faces the displacement in thickness direction is not allowed.

Mesh is formed by hexagonal C3D8R elements with a minimum size of 10 μm around the cutting area and 100 μm at laminate sides, as it is shown in Fig. 2. A small thickness of 50 μm with 5 elements is modelled to reduce considerably the computational cost.

Tool is modelled as a solid rigid to save computational time as its deformation during a machining is negligible. Tool-laminate contact is modelled using the option surface-node surface contact available in Abaqus/Explicit. Additionally, the general contact option available in the software adds an internal friction between the elements surfaces in the cutting area to enhance the model robustness. A constant coulomb friction coefficient of 0.5 is used to model the tool/laminate interaction. Note that, this friction coefficient should vary with fibre orientation as they produce different friction conditions [9]. However, as the study of friction in composite machining is not the scope of this work a constant value employ typically in this kind of investigations is selected [10,11].

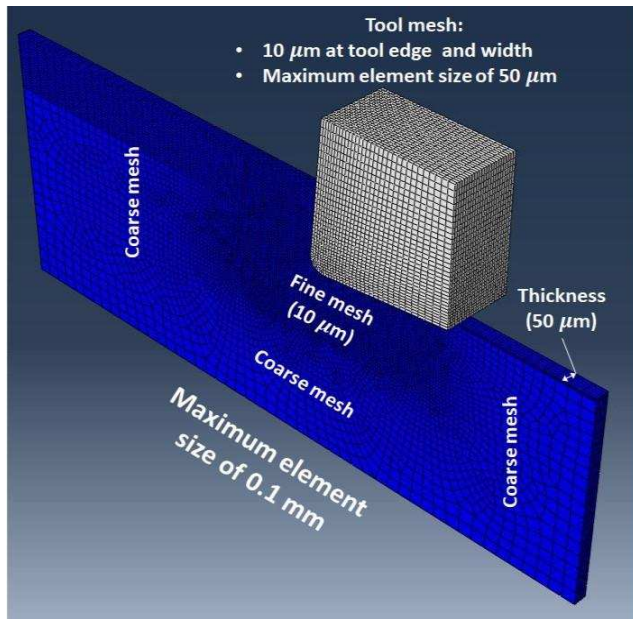


Fig.2.Mesh distribution

3. 3D composite damage model

The composite damage model employed in this work is inserted in the performed explicit analysis via a user-defined fortran subroutine VUMAT. This damage model implements different damage variables which degrade separately the fibre and matrix mechanical properties in the constitutive equations of the material.

The algorithm to reduce composite mechanical properties contains two remarkable phases: (1) damage initiation and (2) damage propagation. More details about these phases are broken down in the below subsections.

3.1. Constitutive equations

Because of the high heterogeneity of composite materials, their constituents should be treated separately to achieve accurate and robust predictions. For this reason, six damage modes which affect to fibre and matrix separately are considered in this study. These damage modes are broken down below.

- d_f = fibre traction damage

- d_{fc} = fibre compression damage
- d_{m2} = in-ply matrix traction damage
- d_{mc2} = in-ply matrix compression damage
- d_{m3} = out-of-plane matrix traction damage
- d_{mc3} = out-of-plane matrix compression damage

However, in the constitutive equations these aforementioned damages are implemented using other damage definitions such as fibre damage (df), matrix damages (dm2 and dm3) and shear damages (ds1, ds2 and ds3). They are allocated in the diagonal of the compliance matrix (S) as it is illustrated in Fig. 3.

3.2. Damage initiation

Reliable predictions of damage initiation are vital for achieving accurate simulations as it determines the initial point where the mechanical properties of a constituent start to decrease. For this purpose, in this work well-establish composite failure criteria have been used such as Hashin's [12] and Puck's [13] failure criteria are used.

To assess the fibre failure the Hashin's failure criteria is selected to start fibre damage in traction and compression states, as read.

- Fibre traction

$$\left(\frac{\sigma_{11}}{X_T}\right)^2 + \left(\frac{\sigma_{12}}{S_{12}}\right)^2 \geq 1 \tag{1}$$

- Fibre compression

$$\left|\frac{\sigma_{11}}{X_C}\right| \geq 1 \tag{2}$$

To predict matrix failure states transversal to the fibre (in-ply) Puck's failure criteria have been selected due to its high capabilities to predict accurate the matrix failure in a large

$$[S]_{3D} = \begin{bmatrix} \frac{1}{E_1(1-d_f)} & -\frac{\nu_{12}}{E_1} & -\frac{\nu_{13}}{E_1} & 0 & 0 & 0 \\ -\frac{\nu_{21}}{E_2} & \frac{1}{E_2(1-d_{m2})} & -\frac{\nu_{23}}{E_2} & 0 & 0 & 0 \\ -\frac{\nu_{31}}{E_3} & -\frac{\nu_{32}}{E_3} & \frac{1}{E_3(1-d_{m3})} & 0 & 0 & 0 \\ 0 & 0 & 0 & \frac{1}{G_{12}(1-d_f)(1-d_{m2})} & 0 & 0 \\ 0 & 0 & 0 & 0 & \frac{1}{G_{23}(1-d_{m2})(1-d_{m3})} & 0 \\ 0 & 0 & 0 & 0 & 0 & \frac{1}{G_{13}(1-d_f)(1-d_{m3})} \end{bmatrix}$$

Fig.3. Compliance matrix employed in the damage algorithm

number of scenarios [14]. This factor becomes crucial in the modelling of composite machining because matrix damage modes are the predominant failure to determine the machining induced damage [15]. Note that Puck's failure criteria formulation is quite complex and most of the terms are not explained in this document because of the lack of space. More interested readers are referred to go to [13] to learn more about this failure criteria.

- Matrix Mode A ($\sigma_{22} \geq 0$)

$$\sqrt{\left(\frac{\sigma_{12}}{R_{\perp\parallel}^A}\right)^2 + \left(1 - \frac{p_{\perp\parallel}^{(+)}}{R_{\perp\parallel}^A} R_{\perp\parallel}^{(+A)}\right)^2 \left(\frac{\sigma_{22}}{R_{\perp\parallel}^{(+A)}}\right)^2} + \frac{p_{\perp\parallel}^{(+)}}{R_{\perp\parallel}^A} \sigma_{22} \geq 1 \quad (3)$$

- Matrix Mode B ($\sigma_{22} < 0$ and $\sigma_{22} > -R_{\perp\parallel}^A$)

$$\sqrt{\left(\frac{\sigma_{12}}{R_{\perp\parallel}^A}\right)^2 + \left(\frac{p}{R}\right)^2 \sigma_{22}^2 + \left(\frac{p}{R}\right) \sigma_{22}} \geq 1 \quad (4)$$

- Matrix Mode C ($\sigma_{22} \leq -R_{\perp\parallel}^A$)

$$\frac{1}{2\left[1 + \left(\frac{p}{R}\right) R_{\perp\parallel}^A\right]} \left[\left(\frac{\sigma_{12}}{R_{\perp\parallel}^A}\right)^2 + \left(\frac{\sigma_{22}}{R_{\perp\parallel}^A}\right)^2 \right] \frac{R_{\perp\parallel}^A}{-\sigma_{22}} \geq 1 \quad (5)$$

For predicting the failure of the matrix in the thickness direction a simple maximum stress failure (Eqs. 6 and 7) criteria is used because of this kind of damage is negligible in this analysis as no force is induced by the tool in an orthogonal cutting operation. However, in other machining operations where the material is cut through thickness this damage becomes relevant and accurate predictions are required [16].

- Matrix traction

$$\frac{\sigma_{33}}{Z_T} \geq 1 \quad (6)$$

- Matrix compression

$$\left| \frac{\sigma_{33}}{Z_C} \right| \geq 1 \quad (7)$$

3.3. Damage propagation

After damage initiation occurs, damage variables are upgraded following the continuum damage mechanics (CDM) theory from 0 (no damage) to 1 (total failure) to reduce the mechanical performance of damaged elements. This work applies a progressive linear energy based degradation which is inferred from Eq. 8 based on the equivalent displacement ($\delta_{I,eq}$) of every element. Initial equivalent displacement ($\delta_{I,eq}^0$) is the displacement registered when damage initiation occurs, while final equivalent displacement ($\delta_{I,eq}^f$) is determined using the fracture energy (G_I^f) of damage mode (I), see Eqs. 9 and 10.

$$d_I = \frac{\delta_{I,eq}^f (\delta_{I,eq} - \delta_{I,eq}^0)}{\delta_{I,eq} (\delta_{I,eq}^f - \delta_{I,eq}^0)} \quad (8)$$

$$\delta_{I,eq}^0 = \frac{\delta_{I,eq}}{F_I} \quad (9)$$

$$\delta_{I,eq}^f = \frac{2G_I^c F_I}{\sigma_{I,eq}} \quad (10)$$

Finally, a remaining stiffness in matrix damage modes and shear damage of a 5% and 20% is inserted to avoid element distortional problems. Additionally, after one element achieves high strain levels -1.2 or superior- in one of the main material directions, it is deleted to allow Abaqus/Explicit continue the simulation.

4. Results and discussion

In order to obtain accurate simulations, the typical partial recovery of the material in composite machining after the tool

passes away (spring back) needs to be taken into account. This effect is considered in this work with the application of a progressive vertical displacement through the below laminate increasing gradually the machining forces without excessive element distortion. This vertical penetration is always in the order of half or one tool edge radius as investigated by Wang et al. [17].

Despite the fact that chip fracture and sub-surface damage are factors intimately related in composite machining, deletion of meshed element to simulate the chip fracture limits the capacity of the model to propagate the damage to the adjacent elements [18]; it reduces the accuracy of the numerical predictions. Due to this fact, the simulation of the chip fracture is not modelled in this work. Therefore, the tool displacement to create the first chip fracture is simulated to accurately emulate the damage in the CFRP laminate at this moment. Same horizontal and vertical displacements used in [8] are employed. These displacements are showcased in Table 4.

Table 4. Tool displacement for every studied fibre orientation

Fibre orientation	Horizontal displacement (mm)	Vertical displacement (mm)
0°	0.0521	0.0313
15°	0.0236	0.0226
30°	0.0381	0.0411
45°	0.0366	0.0395
60°	0.0679	0.0407
75°	0.0439	0.0439
90°	0.0600	0.0600

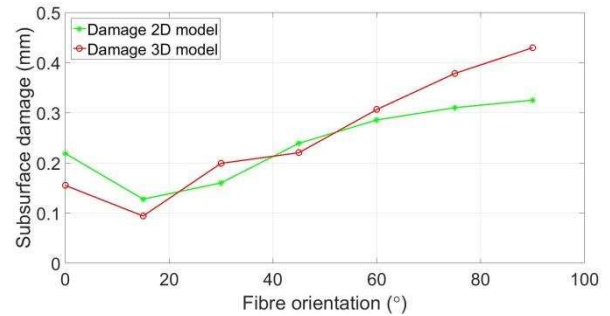


Fig. 4. Subsurface damage predicted in 2D FE models developed by Cepero-Mejias et al. [9] and the results obtained in this work

Note that, the data illustrated in Table 4 is validated with experiments performed on GFRP specimens. From these experiments developed by Bhatnagar et al. [19], the instant before the chip formation is calculated. Later, the sub-surface in CFRP laminates is calculated assuming that chip fracture would take place at the same cutting time than for GFRP laminates due to the similarity of the fracture nature in both materials. Therefore, in order to enhance the quality of the numerical predictions, trials with CFRP specimens are necessary in the future.

As observed in Fig. 4 the main differences between the predictions obtained with the 2D and 3D FE simulations is found for high fibre orientations 75°-90°. These remarkable differences are motivated because of the internal friction between elements in the cutting zone or the limitation of the shear damage aforementioned in section 2 and 3, respectively.

In the case of high fibre orientations, more subsurface damage is predicted with the 3D FE models because the

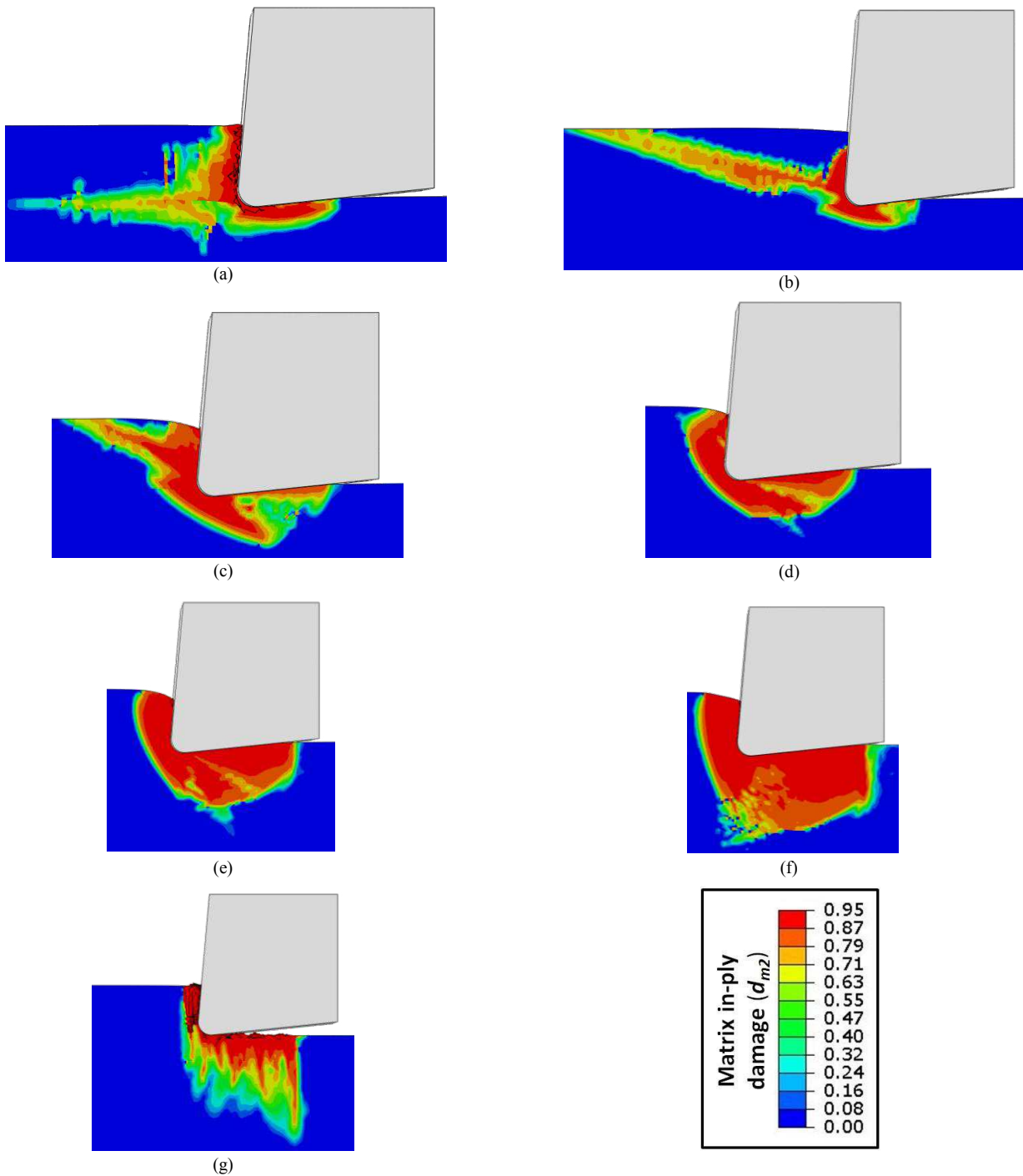


Fig. 5. Representation of the matrix in-ply damage in all simulations developed for fibre orientations: (a) 0°, (b) 15°, (c) 30°, (d) 45°, (e) 60°, (f) 75° and (g) 90°

limitation of shear damage facilitate the vertical propagation of damage avoiding the excessive horizontal damage propagation registered in the predictions with 2D FE models. This excessive horizontal propagation of damage in 2D simulations is produced due to large shear deformations limited the elements stiffness to 0 and the loads are transferred to the adjacent meshed elements abruptly without a progressive transmission.

In addition in the case of 90° the internal friction of elements contribute to predict more realistically the machining conditions than in 2D FE models because there are several elements separated from the rest of the laminate that

are still pushing to the rest of the laminate and they are not free as in the case of 2D simulations.

For 0° fibre orientation, the vertical limitation of damage is observed to be reduced due to the limitations of shear damage which apply the same mechanism explained for the excessive horizontal damage propagation in high fibre orientations. Therefore, it is concluded that the shear damage restrictions should be less restrictive in the simulations with this fibre orientations to obtain similar predictions with respect to the 2D FE model. In general, the machining induced damage is spread in parallel and perpendicular to the fibre directions, excepting for fibre orientations of 60° and 75°

where large damage below the tool is appreciated because of the high spring back modelled in these cases, see Fig. 5.

5. Conclusions

This work offers a novel 3D FE model in composite machining is used for studying the machining induced damage. Numerical predictions are demonstrated to predict similar results found in other publications developed previously by Cepero-Mejías et al. [8]. Note that, to increase the quality of the numerical results obtained in this work, several orthogonal cutting tests need to be performed with CFRP specimens. Well established composite failure criteria such as Hashin's and Puck's proposals are used to predict damage initiation. Subsequently, a continuum damage mechanics (CDM) linear law is applied to account the severity of the damage in the affected area. Internal element friction and limitation of shear damage propose in this study modify the predictions of 2D FE models, reducing damage propagation for low fibre orientations and increasing the subsurface damage predicted in 2D FE analysis for high fibre orientations. In this study a simple case of the orthogonal cutting of UD-CFRP laminates is modelled; however the potential of this investigation is much higher because this numerical approach is able to model the machining of cross ply laminates and also more complex machining operations such as milling, drilling, etc; further investigations in this direction will be performed in the close future.

Acknowledgements

This work is funded by the EPSRC Industrial Doctoral Centre (EP/L016257/1) of Sheffield.

References

- [1] J. Fraga, "Boeing 787 from the Ground Up," *AERO Mag.*, pp. 17–23, 2006.
- [2] K. Kerrigan and R. J. Scaife, "Wet vs dry CFRP drilling: Influence of cutting fluid on tool performance," *Procedia CIRP*, vol. 77, no. Hpc, pp. 315–319, 2018.
- [3] R. M. Saoubi et al., "Manufacturing Technology High performance cutting of advanced aerospace alloys and composite materials," *CIRP Ann. - Manuf. Technol.*, vol. 64, no. 2, pp. 557–580, 2015.
- [4] O. J. Nixon-Pearson and S. R. Hallett, "An experimental investigation into quasi-static and fatigue damage development in bolted-hole specimens," *Compos. Part B Eng.*, vol. 77, pp. 462–473, 2015.
- [5] C. Santiuste, X. Soldani, and M. H. Miguélez, "Machining FEM model of long fiber composites for aeronautical components," *Compos. Struct.*, vol. 92, no. 3, pp. 691–698, 2010.
- [6] J. Xu and M. El Mansori, "Numerical modeling of stacked composite CFRP/Ti machining under different cutting sequence strategies," *Int. J. Precis. Eng. Manuf.*, vol. 17, no. 1, pp. 99–107, 2016.
- [7] S. Zenia, L. Ben Ayed, M. Nouari, and A. Delamézière, "Numerical analysis of the interaction between the cutting forces, induced cutting damage, and machining parameters of CFRP composites," *Int. J. Adv. Manuf. Technol.*, vol. 78, no. 1–4, pp. 465–480, 2015.
- [8] F. Cepero-mejías, J. L. Curiel-sosa, C. Zhang, and V. A. Phadnis, "Effect of cutter geometry on machining induced damage in orthogonal cutting of UD polymer composites : FE study," *Compos. Struct.*, vol. 214, no. February, pp. 439–450, 2019.
- [9] D. Nayak, N. Bhatnagar, and P. Mahajan, "Machining studies of ud-frp composites part 2: Finite element analysis," *Mach. Sci. Technol.*, vol. 9, no. 4, pp. 503–528, 2005.
- [10] L. Lasri, M. Nouari, and M. El Mansori, "Modelling of chip separation in machining unidirectional FRP composites by stiffness degradation concept," *Compos. Sci. Technol.*, vol. 69, no. 5, pp. 684–692, 2009.
- [11] X. Soldani, C. Santiuste, A. Muñoz-Sánchez, and M. H. Miguélez, "Influence of tool geometry and numerical parameters when modeling orthogonal cutting of LFRP composites," *Compos. Part A Appl. Sci. Manuf.*, vol. 42, no. 9, pp. 1205–1216, 2011.
- [12] Z. Hashin, "Failure Criteria for Unidirectional FibreComposites," *J. Appl. Mech.*, vol. 47, no. June, pp. 329–334, 1980.
- [13] A. Puck and H. Schurmann, "Failure Analysis of Frp Laminates By Means of Physically Based Phenomenological Models *," *Compos. Sci. Technol.*, vol. 3538, no. 96, pp. 1633–1662, 1998.
- [14] M. J. Hinton, A. S. Kaddour, and P. D. Soden, "A comparison of the predictive capabilities of current failure theories for composite laminates , judged against experimental evidence," *Compos. Sci. Technol.*, vol. 62, pp. 1725–1797, 2002.
- [15] F. Cepero-Mejías, V. A. Phadnis, and J. L. Curiel-sosa, "Machining induced damage in orthogonal cutting of UD composites : FEA based assessment of Hashin and Puck criteria," *17th CIRP Conf. Model. Mach. Oper.*, vol. 82, pp. 332–337, 2019.
- [16] V. A. Phadnis, F. Makhdum, A. Roy, and V. V. Silberschmidt, "Drilling in carbon / epoxy composites : Experimental investigations and finite element implementation," *Compos. Part A Appl. Sci. Manuf.*, vol. 47, pp. 41–51, 2013.
- [17] X. M. Wang and L. C. Zhang, "An experimental investigation into the orthogonal cutting of unidirectional fibre reinforced plastics," *Int. J. Mach. Tools Manuf.*, vol. 43, no. 10, pp. 1015–1022, 2003.
- [18] C. Santiuste, Díaz-Álvarez, X. Soldani, and H. Miguélez, "Modelling thermal effects in machining of carbon fiber reinforced polymer composites," *Reinf. Plast. Compos.*, vol. 33, no. 8, pp. 758–766, 2014.
- [19] D. Nayak, N. Singh, N. Bhatnagar, and P. Mahajan, "An Analysis of Machining Induced Damages in FRP Composites — A Micromechanics Finite Element Approach," *AIP Conf. Proc.*, vol. 712, pp. 327–331, 2004.